Letter

Evidence of quantum spin liquid state in a Cu^{2+}-based $S = \frac{1}{2}$ triangular lattice antiferromagnet

K. Bhattacharya,[1] S. Mohanty,[2] A. D. Hillier,[3] M. T. F. Telling,[3] R. Nath,[2] and M. Majumder[1,*]

[1] *Department of Physics, Shiv Nadar Institution of Eminence, Gautam Buddha Nagar, UP 201314, India*
[2] *School of Physics, Indian Institute of Science Education and Research, Thiruvananthapuram 695551, India*
[3] *ISIS Facility, STFC Rutherford Appleton Laboratory, Chilton, Oxfordshire OX11 0QX, United Kingdom*

(Received 8 May 2024; revised 19 June 2024; accepted 13 July 2024; published 5 August 2024)

The layered triangular lattice owing to 1 : 2 order of B and B' sites in the triple perovskite $A_3BB'_2O_9$ family provides an enticing domain for exploring the complex phenomena of quantum spin liquids (QSLs). We report a comprehensive investigation of the ground-state properties of $Sr_3CuTa_2O_9$ that belongs to the above family by employing magnetization, specific heat, and muon spin relaxation (μSR) experiments down to the lowest temperature of 0.1 K. Analysis of the magnetic susceptibility indicates that the spin lattice is a nearly isotropic $S = 1/2$ triangular lattice. We illustrate the observation of a gapless QSL in which conventional spin ordering or freezing effects are absent, even at temperatures more than two orders of magnitude smaller than the exchange energy ($J_{\mathrm{CW}}/k_{\mathrm{B}} \simeq -5.04$ K). Magnetic specific heat in zero field follows a power law, $C_{\mathrm{m}} \sim T^{\eta}$, below 1.2 K with $\eta \approx 2/3$, which is consistent with a theoretical proposal of the presence of a spinon Fermi surface. Below 1.2 K, the μSR relaxation rate shows no temperature dependence, suggesting persistent spin dynamics, as expected for a QSL state. Delving deeper, we also analyze longitudinal field μSR spectra, revealing strong dynamical correlations in the spin-disordered ground state. All of these highlight the characteristics of spin entanglement in the QSL state.

DOI: 10.1103/PhysRevB.110.L060403

Introduction. Quantum spin liquid (QSL) is an exotic and highly entangled quantum state with no spontaneous symmetry breaking down to absolute zero temperature, despite strong correlations among spins. Such a quantum phase is characterized by an emergent gauge field and fractional excitations called spinons [1,2]. This state was first theoretically predicted by P. W. Anderson as a resonating valance bond (RVB) state for interacting Heisenberg spins in a two-dimensional (2D) triangular lattice antiferromagnet (TLAF) [3]. Subsequently, it was recognized that the true ground state of the isotropic Heisenberg TLAF is a three-sublattice 120° Néel order [4,5]. Thereafter, considerable effort has been dedicated to stabilizing the QSL state in a Heisenberg TLAF. For instance, (i) in an isotropic TLAF with Heisenberg interactions, the competing nearest-neighbor (NN) (J_1) and next-nearest-neighbor (NNN) (J_2) interactions can stabilize a gapless Dirac QSL state for $0.08 \lesssim J_2/J_1 \lesssim 0.16$ that is sandwiched between the 120° Néel order and stripe state in the phase diagram [6,7]. A tiny J_3 can also destabilize the magnetic long-range order (LRO), leading to a QSL phase in this model [8]. However, there are theoretical results that illustrate the importance of third nearest-neighbor exchange coupling (J_3) to achieve a QSL state [9]. (ii) Considering spatially anisotropic Heisenberg interactions (J and J'), two different types of QSL states are favored: gapless QSL for $J'/J \lesssim 0.65$ and gapped QSL for $0.65 \lesssim J'/J \lesssim 0.8$ [10].

Over the years, the pursuit of new TLAFs with low spin values (e.g., $S = 1/2$) has become a focal area of research, as it is believed that QSL is a manifestation of enhanced quantum fluctuations and magnetic frustration. However, the experimental realization of QSL in $S = 1/2$ Heisenberg TLAFs is scarce due to the availability of limited model materials. Typically, the majority of the Heisenberg TLAFs show magnetic LRO at finite temperatures due to the interlayer couplings and exchange anisotropy which are inherently present in real materials [11–17]. To the best of our knowledge, as far as inorganic compounds are concerned, QSL in a Cu^{2+}-based $S = 1/2$ Heisenberg TLAF is realized only in $Sr_3CuSb_2O_9$ [18], reported to date. Note that $Ba_3CuSb_2O_9$ likewise exhibits a QSL ground state; however, there is still disagreement over the arrangement of Cu^{2+} ions, specifically whether it is triangular or Honeycomb [19–21]. $Sr_3CuSb_2O_9$ belongs to the triple perovskite family. The family of triple perovskite ($A_3BB'_2O_9$ with A = Sr/Ba, B = Cu/Ca/Te/Os, B' = Sb/Ru/Ir/Fe) [20,22–25] compounds is interesting, since some of the family members have 1 : 2 ordering of B/B' sites, owing to the site sharing of B and B' elements [22,23]. Depending on their crystal structure and space group, the B site could form a superlattice structure with a specific propagation vector. For $Sr_3CuSb_2O_9$, Kundu *et al.* have shown that it forms a superlattice structure with a propagation vector $(\frac{1}{3}, \frac{1}{3}, \frac{1}{3})$ and effectively forms an edge-shared triangular lattice on the (111) plane. In this pseudocubic system, the Cu^{2+} and Sb^{5+} planes are present in 1 : 2 order and the compound evinces a QSL state [18]. Thus, this family of compounds holds great potential to showcase quantum magnetism due to frustration. With this motivation, we investigated the ground state of another member of this family, $Sr_3CuTa_2O_9$ (SCTO), where the $S = 1/2$ moments are embedded in an edge-shared triangular lattice. From a detailed experimental investigation, by employing magnetization, specific heat, and muon spin relaxation/rotation (μSR)

*Contact author: mayukh.majumder@snu.edu.in

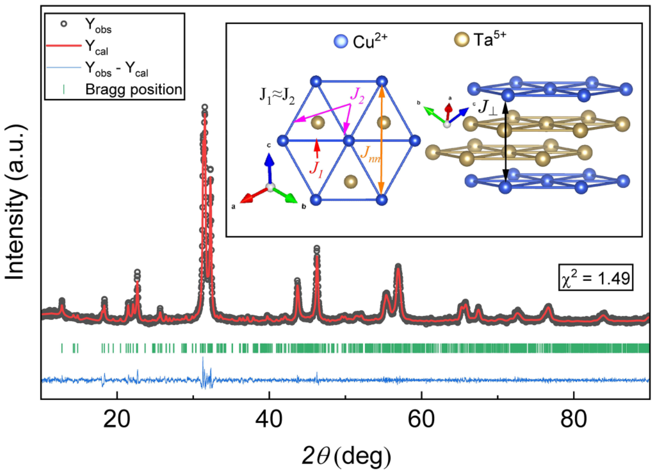

FIG. 1. Rietveld refinement of the powder XRD pattern taking the space group $P\bar{1}$. Inset: Cu layers arranged in a triangular lattice. The possible nearest-neighbor (J_1 and J_2), next-nearest-neighbor (J_{nn}), and interplane ($J_\perp$) exchange couplings are illustrated.

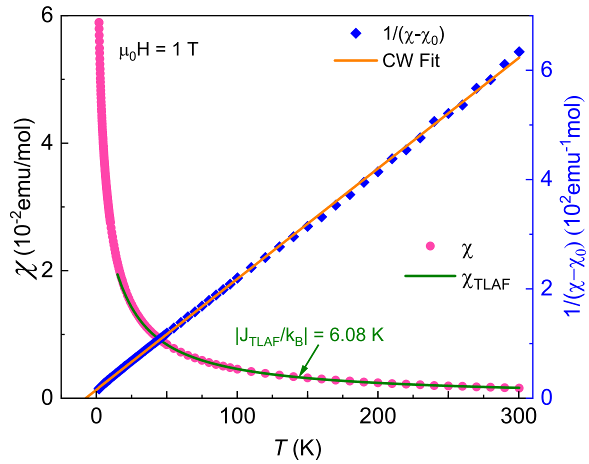

FIG. 2. Left y-axis: χ as a function of T measured at $\mu_0 H = 1$ T. The solid line represents the fit using an anisotropic ($J_1 - J_2$) $S = 1/2$ TLAF model [Eq. (1)]. Right y-axis: Inverse susceptibility (after subtracting χ_0) as a function of T at $\mu_0 H = 1$ T, and solid line is the Curie-Weiss fit.

techniques, we provide solid evidence of a gapless QSL state in SCTO. This compound serves as a model isotropic edge-shared TLAF that hosts QSL.

Powder x-ray diffraction. A polycrystalline SCTO sample was synthesized following the procedure described in the Supplemental Material (SM) [26]. Rietveld refinement of the powder x-ray diffraction (XRD) pattern of SCTO at room temperature was carried out assuming a tetragonal space group $P4/mmm$ (No. 123) with lattice parameters $a = b = 3.93$ and $c = 4.14$ Å, which is a pseudocubical structure (details are in SM [26]). The best refinement was achieved with a goodness-of-fit $\chi^2 \sim 5.06$. Some peaks at lower angles ($2\theta < 30^\circ$) could not be indexed with this space group, as shown in the SM [26]. These peaks correspond to a k value of $\frac{1}{3}(111)$. Thus, these peaks are associated with the superlattice structure owing to the intersite mixing of Cu^{2+}/Ta^{5+} with occupancies $\frac{1}{3}/\frac{2}{3}$ and form a 1 : 2 order, which is common in these triple perovskite systems. Note that the presence of superlattice structure is dependent on the synthesis conditions [27]. Superlattice peaks along with Bragg peaks of the $P4/mmm$ space group are well fitted with a lower symmetric triclinic space group $P\bar{1}$ (yield a goodness-of-fit $\chi^2 \sim 1.49$), as shown in Fig. 1. The 1 : 2 site ordering with propagation vector $\frac{1}{3}(111)$ in a pseudocubic structure forms a layered edged-shared triangular lattice of Cu^{2+} in the (111) plane. The two successive triangular layers of Cu^{2+} are separated by two layers of Ta^{5+}, as shown in the inset of Fig. 1. A similar structure is also found in $Sr_3CuSb_2O_9$ [18]. Note that the Cu^{2+} moments form an edge-shared bilateral or quasi-equilateral triangle with a very small difference in the bond lengths (5.56, 5.70, and 5.70 Å) along the edges of the triangle. The smallest bond length between interplane Cu^{2+} ions is about ∼6.93 Å.

Magnetization. Temperature-dependent dc magnetic susceptibility $\chi(T)(\equiv M/H)$ measured at $\mu_0 H = 1$ T is depicted in Fig. 2. χ increases monotonically with lowering temperature, and no anomaly associated with magnetic LRO is observed down to 1.85 K. $\chi(T)$ measured in zero-field-cooled and field-cooled protocols in a low magnetic field (50 Oe) shows no bifurcation down to 1.85 K [26], ruling out a spin-glass-like transition. In Fig. 2 we fitted the $\chi(T)$ data in high temperatures ($T > 100$ K) by the modified Curie-Weiss (CW) law [$\chi(T) = \chi_0 + C/(T - \theta_{CW})$] that yields temperature-independent susceptibility $\chi_0 \simeq -2.18 \times 10^{-5}$ emu/mol Cu^{2+}, Curie constant $C \simeq 0.49$ emu K/mol Cu^{2+}, and characteristic CW temperature $\theta_{CW} \simeq -7.56 \pm 0.11$ K. The negative sign of θ_{CW} indicates dominant antiferromagnetic (AFM) interaction between Cu^{2+} spins. From the value of C, the effective moment is estimated to be $\mu_{\rm eff} = \sqrt{3k_B C/N_A} \simeq 1.97(8)\,\mu_B/Cu^{2+}$ (where k_B, N_A, μ_B, and g are the Boltzmann constant, Avogadro's number, Bohr magneton, and Landé g factor, respectively). This value is indeed comparable with the expected value of $\mu_{\rm eff} \simeq 1.73\,\mu_B/Cu^{2+}$ [$= g\sqrt{S(S+1)}\mu_B$] for Cu^{2+} ($S = 1/2$). Here, θ_{CW} represents the overall energy scale of the exchange couplings, and one can estimate the average intralayer coupling (J_{CW}/k_B) as $\theta_{CW} = -zJ_{CW}S(S+1)/3k_B$. Taking the experimental value of θ_{CW} and the number of NN spins $z = 6$ for a 2D-TLAF, we got $J_{CW}/k_B \simeq -5.04$ K.

As inferred from the crystal structure, one expects a spatial anisotropy in the triangular unit due to a slightly varying bond length. Therefore, to analyze $\chi(T)$ we fitted the data in the high-temperature region ($T > 100$ K) by $\chi(T) = \chi_0 + \chi_{\rm TLAF}(T)$. $\chi_{\rm TLAF}$ is the expression of high-temperature series expansion (HTSE) for a $S = 1/2$ 2D spatially anisotropic TLAF which has the form [28]

$$\chi_{\rm TLAF} = \frac{N_A g^2 \mu_B^2}{k_B T} \times \sum_{\rm n=0} \left(\frac{J_2}{T}\right)^{\rm n} \sum_{\rm m=0}^{\rm n} \frac{c_{\rm m,n} y^{\rm m}}{4^{\rm n+1}{\rm n}!}. \quad (1)$$

Here, $y = J_1/J_2$, with J_1 and J_2 representing the NN and NNN exchange interactions, respectively. The integer coefficients $c_{m,n}$ are given in Ref. [28]. By fixing the χ_0 value (obtained from CW fit), the fit yields $J_2/k_B = (6.08 \pm 0.35)$ K, and $J_2/J_1 \simeq 1$. The value $J_2/J_1 \simeq 1$ indicates an effective equilateral triangular lattice as far as the strength of exchange interactions is concerned. Moreover, the obtained value of

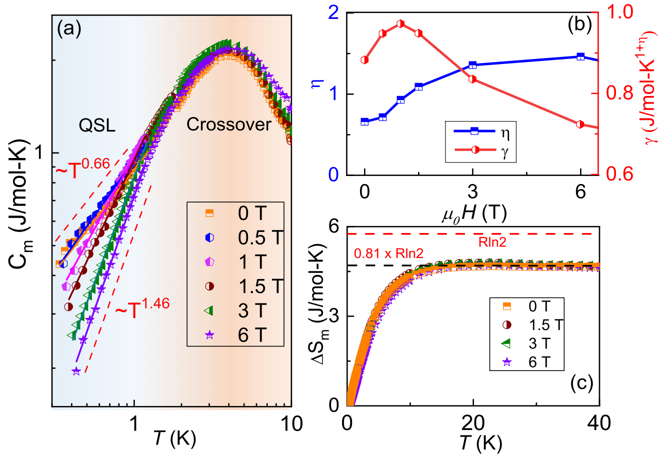

FIG. 3. (a) Magnetic specific heat (C_m) as a function of T for different fields. The solid lines are the fits using $C_m \sim \gamma T^{\eta}$, and red dashed lines correspond to $T^{0.66}$ and $T^{1.46}$. (b) Variation of η and γ with the magnetic field. (c) Magnetic entropy (ΔS_m) as a function of T, and the dotted lines mark the theoretically expected and experimentally observed values of entropy.

J_2/k_B is in good agreement with J_{CW}/k_B, further endorsing a nearly isotropic triangular lattice. We also fitted the $\chi(T)$ data by the HTSE of a $S = 1/2$ isotropic TLAF that uses the Padé approximation [26]. The fit results in nearly identical exchange coupling, $J_{iso}/k_B = (6.09 \pm 0.40)$ K.

Specific heat. Specific heat not only provides information about magnetic LRO but also the low-energy excitations of a spin system. Specific heat data in zero field, as well as in applied fields, show the absence of a λ-type anomaly reminiscent of a magnetic LRO down to 0.33 K. To extract the magnetic contribution to the specific heat (C_m), we have subtracted the lattice contribution (C_{lat}) from the total specific heat (C_p). The lattice contribution was estimated considering both the Debye and Einstein models in the temperature range of 30–190 K, with one Debye and two Einstein terms (see SM) [26]. C_m vs T presented in Fig. 3(a) features a broad hump at around ~4 K (T_{hump}), which indicates crossover from a thermally disordered paramagnet to a quantum paramagnetic QSL state, typically observed in QSL systems [29,30]. Moreover, for a Heisenberg TLAF, such a hump is expected at $T_{hump}/J \simeq 0.55$ [31], which yields $J/k_B \approx 7.27$ K, consistent with the J one evaluated from the magnetization data. For $T \leqslant 1.2$ K, C_m measured in zero field follows a power-law behavior $C_m \sim \gamma T^{\eta}$ with $\eta = 2/3$. For different gapless QSL candidates, C_m usually follows either linear ($\eta = 1$) [20,32] or quadratic ($\eta = 2$) [18,33] behavior as a function of temperature, whereas for SCTO, $\eta = 2/3$ and interestingly, is indeed consistent with a theoretical prediction for an equilateral TLAF with the presence of a gapless Fermi surface as $C_m \sim k_B \nu_0 t_{spinon}^{1/3} (k_B T)^{2/3}$. Here, ν_0 is the density of states at the spinon Fermi surface, and t_{spinon} is the spinon hopping amplitude [34]. The obtained field dependences of η and γ are shown in Fig. 3(b). With the application of a magnetic field, the exponent η grows slowly, probably due to the gradual suppression of 2D quantum correlations. We also calculated the magnetic entropy change (ΔS_m) for different fields as shown in Fig. 3(c). ΔS_m recovers only ~81% of Rln2 above 10 K. This is a common signature of a frustrated magnets, where entropy is released over a broad temperature range [35–37]. The remaining 19% of entropy will be released at further low temperatures reflecting the persistence of a strong correlation among Cu^{2+} spins present at further low temperatures.

In addition, we have also measured temperature-dependent thermal conductivity $\kappa(T)$ down to $T = 2$ K in different magnetic fields (see SM) [26]. The low-temperature data are fitted by $\kappa/T = a + bT^2$, which yields a nonzero intercept $a \simeq 0.0211$ mW K^{-2} cm^{-1}, which further corroborate a gapless QSL state with a finite spinon density of states. However, a detailed quantitative analysis and solid evidence of QSL from thermal conductivity measurements require data at ultralow temperatures.

Muon spin relaxation (μSR). Being sensitive to a local internal magnetic field as small as 0.1 Oe, μSR is an ideal microscopic tool to probe magnetic LRO. In addition, μSR can distinguish between static and dynamic correlations among the spins, making it a powerful tool to uncover the putative QSL behavior. Hence, to elucidate the magnetic ground state of SCTO, we collected μSR data in zero field (ZF) condition as a function of temperature, as well as in longitudinal fields (LFs), at the base temperature of 0.1 K. In the following, we delineate our observations from the μSR data.

(i) ZF μSR asymmetries displayed in Fig. 4(a) confirm the absence of magnetic LRO down to 0.1 K, as they decay continuously without any oscillations or initial asymmetry drop [Fig. 4(a)]. The ZF μSR asymmetries are well fitted by a stretch exponential function with an extra background term B_{bg} (owing to some muons missing the sample and placed at the Ag-sample holder and the cryostat wall) [38]:

$$P(t) = P(0) \exp(-\lambda t)^{\beta} + B_{bg}. \tag{2}$$

Here, $P(0) \sim 0.28$ (weakly temperature and field dependent) is the initial asymmetry, λ is the relaxation rate, and β is the stretching exponent. While fitting the ZF μSR asymmetries, $B_{bg} \approx 0.08$ is kept constant for all the temperatures. The obtained fitting parameters (λ_{ZF} and β_{ZF}) are plotted in Figs. 4(b) and 4(c).

(ii) In the high-temperature ($T > 10$ K) paramagnetic regime, the uncorrelated Cu^{2+} spins fluctuate rapidly and randomly. The fluctuation rate can be calculated using the strength of exchange coupling ($J/k_B \simeq 5.04$ K) as $\nu = \sqrt{z} J s/\hbar \sim 1.6 \times 10^{10}$ Hz [39,40], where ν is the spin fluctuation rate and $z = 6$ is the coordination number for a 2D TLAF. λ_{ZF} (at $T > 10$ K) can provide an idea about the local internal field distribution (Δ) based on the Redfield formula [41], $\lambda(T \geqslant 10\,K, H) = 2\Delta^2\nu/(\nu^2 + \gamma_\mu^2 \mu_0^2 H^2)$, which yields $\Delta \sim 5.1 \times 10^7$ Hz. This confirms the fast-fluctuation limit ($\Delta \ll \nu$) [40,42] is responsible for the temperature-independent relaxation rate in the high-temperature range. With lowering the temperature, the relaxation rate λ_{ZF} starts increasing below $T \leqslant 10$ K, which implies slowing down of fluctuating moments due to the growth of correlations among the Cu^{2+} spins [42,43]. This temperature regime is marked as the crossover region from a paramagnetic to QSL state in Fig. 4(b), consistent with the broad hump observed in $C_m(T)$ [see Fig. 3(a)]. With further lowering in temperature,

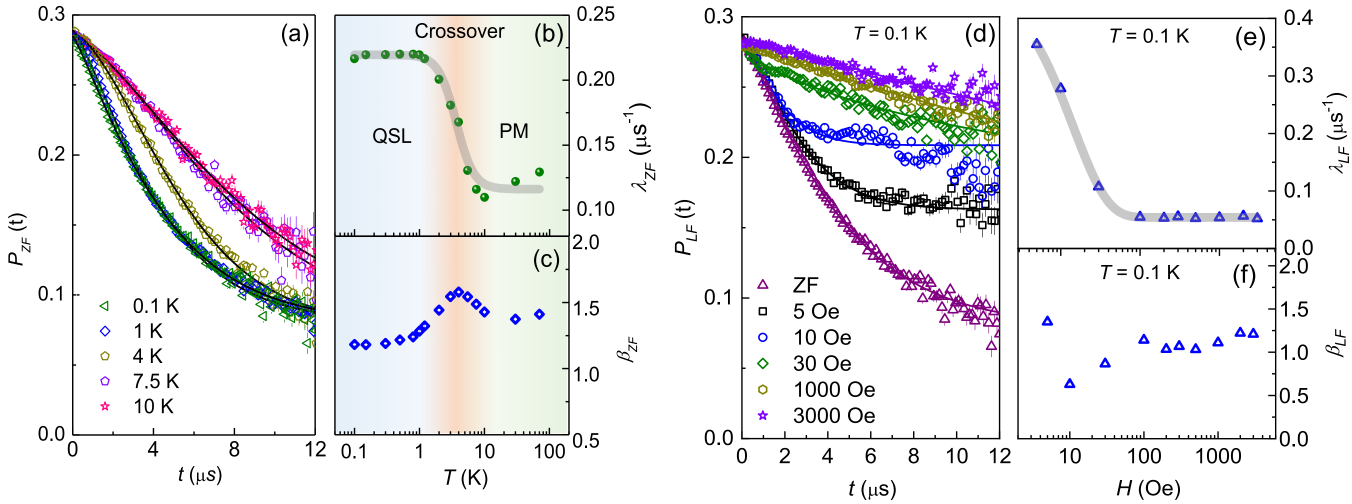

FIG. 4. (a) ZF-μSR asymmetry spectra as a function of t for different temperatures. Solid lines are the fits using Eq. (2). (b) ZF relaxation rate (λ_{ZF}) vs T. (c) β_{ZF} as a function of T. The orange-shaded region represents the crossover region ($1.2 \leqslant T \leqslant 10$ K) from paramagnetic to the QSL state. (d) μSR asymmetry spectra measured in different longitudinal fields at $T = 0.1$ K, and the solid lines represent the fits using Eq. (2). (e) The corresponding relaxation rate λ_{LF} as a function of the longitudinal field. (f) β_{LF} as a function of the longitudinal field.

λ_{ZF} becomes temperature independent (for $T \leqslant 1.2$ K), indicating the persistence of spin dynamics. This persistent spin dynamics is considered to be a generic feature of QSL, as reported for other celebrated QSL candidates [18,29,38,44]. It is interesting to note that the saturation of λ_{ZF} below $\sim$1.2 K exactly coincides with the temperature range where $C_m(T)$ follows a power-law behavior. Thus, the behavior of $\lambda_{ZF}(T)$ along with the power-law dependency of $C_m(T)$ provides a robust signature of QSL at low temperatures.

(iii) LF μSR experiments are performed to explore the nature of the spin dynamics at low temperatures. LF-μSR asymmetry spectra measured in different fields at $T = 0.1$ K are shown in Fig. 4(d). They are fitted well by Eq. (2). The obtained field dependencies of λ_{LF} and β_{LF} are depicted in Figs. 4(e) and 4(f), respectively. The quick suppression of λ_{LF} below 100 Oe reflects the decoupling of the nuclear contribution to the relaxation rate [44,45]. More interestingly, above 0.01 T, the remaining $\lambda_{LF} \sim 0.05\,\mu\text{s}^{-1}$, originating from the electronic contribution, is almost field independent up to an LF of 3000 Oe. At low temperatures ($T \leqslant 1.2$ K), if we assume that the relaxation process in the plateau regime of λ_{ZF} is due to a static local field, then it would correspond to $\sim$0.25 mT (as $B_{loc} = \lambda/\gamma_\mu$, where $\gamma_\mu = 2\pi \times 135.5\,s^{-1}\,\mu\text{T}^{-1}$ is the gyromagnetic ratio of muons). In such a scenario, an LF of 750 Oe, which is 5 times larger than B_{loc} would be sufficient to decouple the relaxation channel. On the contrary, even in an LF of 3000 Oe, the decoupling of the relaxation channel was not achieved. One may require higher LFs to completely decouple the relaxation channel [46]. This observation demonstrates that the correlation among the spins is entirely dynamic (not static) in nature, as expected for a QSL state [18,38,47–49].

(iv) Typically, in a spin-glass state, the value of β is predicted to be about 1/3 [50,51]. On the contrary, the obtained β value shown in Fig. 4(c) attains a constant value of $\sim$1.2 below the crossover region. Furthermore, the magnitude of λ_{ZF} ($\sim 0.12\,\mu\text{s}^{-1}$ at $T \geqslant 10$ K) becomes double ($\sim 0.22\,\mu\text{s}^{-1}$ at $T \leqslant 1$ K) upon cooling the system below the crossover regime, which is also in contrast to that expected for a spin-glass-type transition, where the relaxation rate should increase by few orders of magnitude [40,52]. These observations rule out the possibility of a spin-glass state.

It is important to highlight that the system does not order down to $T_{min} \sim 0.1$ K, which sets the lower limit of the frustration parameter $f = \theta_{CW}/T_{min} \simeq 76$, characterizing SCTO a highly frustrated magnet. Specific heat and μSR results establish a highly dynamic ground state with spinon excitations and a footprint of gapless QSL. The analysis of magnetic susceptibility suggests that the system can be treated as an isotropic TLAF with Heisenberg interactions. In such a scenario, the ground state is expected to be a 120° Néel order rather than a QSL state, if only the NN couplings are considered. Further, despite partial site occupancy, the Cu and Ta sites are arranged periodically with 1 : 2 order, forming separate layers of Cu^{2+} with a triangular lattice. This ensures the minimal effect of disorder driving QSL state. Note that systems with disorder may stabilize random-singlet states, which exhibit scaling behavior in their physical properties, as observed in different compounds with site disorder [53–55]. However, as expected, the physical properties of SCTO do not show any such scaling behavior. All these observations reflect the possible role of NNN interaction (J_{nn}) or interlayer interaction ($J_\perp$) [inset (b) of Fig. 1] in stabilizing the gapless QSL state. Nevertheless, the inelastic neutron scattering experiments on a good-quality single crystal would be essential to shed light on this issue.

Conclusion. In summary, our studies divulge that the Cu^{2+} and Ta^{5+} ions feature a precisely calibrated 1 : 2 site ordering, resulting in separate planes of Cu^{2+} moments with propagation vector $k = \frac{1}{3}(111)$, which creates an effective equilateral triangular lattice. Magnetic susceptibility data agree well with the isotropic $S = 1/2$ TLAF model with a leading exchange coupling of $J/k_B \simeq 6.09$ K. Specific heat data suggest the absence of magnetic LRO down to 0.33 K and provide evidence for spinon excitations. The absence of magnetic LRO was further corroborated by the μSR data measured down to 0.1 K, setting a very high degree of magnetic frustration ($f > 76$) in SCTO. From the μSR analysis, the ground state is found to be a highly dynamic state with no static order, a hallmark of QSL. Thus our detailed investigation unambiguously established that SCTO is one of the rare examples of a gapless QSL realized in a $S = 1/2$ Cu^{2+}-based Heisenberg TLAF. The onset of such a gapless QSL is anticipated to be due to the complex interplay of different exchange couplings (NN and interactions beyond NN). We believe that our results would instigate further experimental as well as theoretical investigations to settle the origin of the emergence of QSL in SCTO.

Acknowledgments. K.B. and M.M. would like to thank the Department of Science and Technology, India, for access to the experimental facility and financial support for the experiment conducted at ISIS muon source [56] and Jawaharlal Nehru Centre for Advanced Scientific Research (JNCASR) for managing the project. S.M. and R.N. would like to acknowledge SERB, India, bearing sanction Grant No. CRG/2022/000997. K.B. and M.M. also thank I. Ishant for fruitful discussions.

[1] L. Balents, Spin liquids in frustrated magnets, Nature (London) **464**, 199 (2010).
[2] T. Lancaster, Quantum spin liquids, Contemp. Phys. **64**, 127 (2023).
[3] P. Anderson, Resonating valence bonds: A new kind of insulator? Mater. Res. Bull. **8**, 153 (1973).
[4] D. A. Huse and V. Elser, Simple variational wave functions for two-dimensional Heisenberg spin-$\frac{1}{2}$ antiferromagnets, Phys. Rev. Lett. **60**, 2531 (1988).
[5] T. Jolicoeur and J. C. Le Guillou, Spin-wave results for the triangular Heisenberg antiferromagnet, Phys. Rev. B **40**, 2727 (1989).
[6] N. E. Sherman, M. Dupont, and J. E. Moore, Spectral function of the $J_1 - J_2$ Heisenberg model on the triangular lattice, Phys. Rev. B **107**, 165146 (2023).
[7] M. Drescher, L. Vanderstraeten, R. Moessner, and F. Pollmann, Dynamical signatures of symmetry-broken and liquid phases in an $S = \frac{1}{2}$ Heisenberg antiferromagnet on the triangular lattice, Phys. Rev. B **108**, L220401 (2023).
[8] J. Merino, M. Holt, and B. J. Powell, Spin-liquid phase in a spatially anisotropic frustrated antiferromagnet: A Schwinger boson mean-field approach, Phys. Rev. B **89**, 245112 (2014).
[9] Y.-F. Jiang and H.-C. Jiang, Nature of quantum spin liquids of the $S = \frac{1}{2}$ Heisenberg antiferromagnet on the triangular lattice: A parallel DMRG study, Phys. Rev. B **107**, L140411 (2023).
[10] S. Yunoki and S. Sorella, Two spin liquid phases in the spatially anisotropic triangular Heisenberg model, Phys. Rev. B **74**, 014408 (2006).
[11] S. Lal, S. J. Sebastian, S. S. Islam, M. P. Saravanan, M. Uhlarz, Y. Skourski, and R. Nath, Double magnetic transitions and exotic field-induced phase in the triangular lattice antiferromagnets $Sr_3Co(Nb, Ta)_2O_9$, Phys. Rev. B **108**, 014429 (2023).
[12] N. Li, Q. Huang, X. Y. Yue, W. J. Chu, Q. Chen, E. S. Choi, X. Zhao, H. D. Zhou, and X. F. Sun, Possible itinerant excitations and quantum spin state transitions in the effective spin-1/2 triangular-lattice antiferromagnet $Na_2BaCo(PO_4)_2$, Nat. Commun. **11**, 4216 (2020).
[13] Y. Kamiya, L. Ge, T. Hong, Y. Qiu, D. L. Quintero-Castro, Z. Lu, H. B. Cao, M. Matsuda, E. S. Choi, C. D. Batista, M. Mourigal, H. D. Zhou, and J. Ma, The nature of spin excitations in the one-third magnetization plateau phase of $Ba_3CoSb_2O_9$, Nat. Commun. **9**, 2666 (2018).
[14] K. Yokota, N. Kurita, and H. Tanaka, Magnetic phase diagram of the $S = \frac{1}{2}$ triangular-lattice Heisenberg antiferromagnet $Ba_3CoNb_2O_9$, Phys. Rev. B **90**, 014403 (2014).
[15] Y. Kojima, M. Watanabe, N. Kurita, H. Tanaka, A. Matsuo, K. Kindo, and M. Avdeev, Quantum magnetic properties of the spin-$\frac{1}{2}$ triangular-lattice antiferromagnet $Ba_2La_2CoTe_2O_{12}$, Phys. Rev. B **98**, 174406 (2018).
[16] K. M. Ranjith, R. Nath, M. Skoulatos, L. Keller, D. Kasinathan, Y. Skourski, and A. A. Tsirlin, Collinear order in the frustrated three-dimensional spin $-\frac{1}{2}$ antiferromagnet $Li_2CuW_2O_8$, Phys. Rev. B **92**, 094426 (2015).
[17] K. M. Ranjith, R. Nath, M. Majumder, D. Kasinathan, M. Skoulatos, L. Keller, Y. Skourski, M. Baenitz, and A. A. Tsirlin, Commensurate and incommensurate magnetic order in spin-1 chains stacked on the triangular lattice in $Li_2NiW_2O_8$, Phys. Rev. B **94**, 014415 (2016).
[18] S. Kundu, A. Shahee, A. Chakraborty, K. M. Ranjith, B. Koo, J. Sichelschmidt, M. T. F. Telling, P. K. Biswas, M. Baenitz, I. Dasgupta, S. Pujari, and A. V. Mahajan, Gapless quantum spin liquid in the triangular system $Sr_3CuSb_2O_9$, Phys. Rev. Lett. **125**, 267202 (2020).
[19] N. Katayama, K. Kimura, Y. Han, J. Nasu, N. Drichko, Y. Nakanishi, M. Halim, Y. Ishiguro, R. Satake, E. Nishibori, M. Yoshizawa, T. Nakano, Y. Nozue, Y. Wakabayashi, S. Ishihara, M. Hagiwara, H. Sawa, and S. Nakatsuji, Absence of Jahn-Teller transition in the hexagonal $Ba_3CuSb_2O_9$ single crystal, Proc. Natl. Acad. Sci. USA **112**, 9305 (2015).
[20] H. D. Zhou, E. S. Choi, G. Li, L. Balicas, C. R. Wiebe, Y. Qiu, J. R. D. Copley, and J. S. Gardner, Spin liquid state in the $S = 1/2$ triangular lattice $Ba_3CuSb_2O_9$, Phys. Rev. Lett. **106**, 147204 (2011).
[21] S. Nakatsuji, K. Kuga, K. Kimura, R. Satake, N. Katayama, E. Nishibori, H. Sawa, R. Ishii, M. Hagiwara, F. Bridges, T. U. Ito, W. Higemoto, Y. Karaki, M. Halim, A. A. Nugroho, J. A. Rodriguez-Rivera, M. A. Green, and C. Broholm, Spin-orbital short-range order on a honeycomb-based lattice, Science **336**, 559 (2012).
[22] D. C. Wallace and T. M. McQueen, New honeycomb iridium(v) oxides: $NaIrO_3$ and $Sr_3CaIr_2O_9$, Dalton Trans. **44**, 20344 (2015).
[23] J. T. Rijssenbeek, S. Malo, V. Caignaert, and K. R. Poeppelmeier, Site and oxidation-state specificity yielding dimensional control in perovskite ruthenates, J. Am. Chem. Soc. **124**, 2090 (2002).
[24] Y. Tang, E. C. Hunter, P. D. Battle, R. P. Sena, J. Hadermann, M. Avdeev, and J. Cadogan, Structural chemistry and magnetic properties of the perovskite $Sr_3Fe_2TeO_9$, J. Solid State Chem. **242**, 86 (2016).

[25] G. S. Thakur, T. C. Hansen, W. Schnelle, S. Guo, O. Janson, J. van den Brink, C. Felser, and M. Jansen, Buckled Honeycomb lattice compound $Sr_3CaOs_2O_9$ exhibiting antiferromagnetism above room temperature, Chem. Mater. **34**, 4741 (2022).

[26] See Supplemental Material at http://link.aps.org/supplemental/10.1103/PhysRevB.110.L060403 for further details about sample preparation, experimental conditions, x-ray diffraction, magnetic susceptibility analysis, estimation of lattice heat capacity, and thermal conductivity data analysis, which also includes Refs. [57–62].

[27] I. Levin, L. Bendersky, J. Cline, R. Roth, and T. Vanderah, Octahedral tilting and cation ordering in perovskite-like $Ca_4Nb_2O_9 = 3{\cdot}Ca(Ca_{1/3}Nb_{2/3})O_3$ polymorphs, J. Solid State Chem. **150**, 43 (2000).

[28] W. Zheng, R. R. P. Singh, R. H. McKenzie, and R. Coldea, Temperature dependence of the magnetic susceptibility for triangular-lattice antiferromagnets with spatially anisotropic exchange constants, Phys. Rev. B **71**, 134422 (2005).

[29] T. Dey, M. Majumder, J. C. Orain, A. Senyshyn, M. Prinz-Zwick, S. Bachus, Y. Tokiwa, F. Bert, P. Khuntia, N. Büttgen, A. A. Tsirlin, and P. Gegenwart, Persistent low-temperature spin dynamics in the mixed-valence iridate $Ba_3InIr_2O_9$, Phys. Rev. B **96**, 174411 (2017).

[30] Y. Li, H. Liao, Z. Zhang, S. Li, F. Jin, L. Ling, L. Zhang, Y. Zou, L. Pi, Z. Yang, J. Wang, Z. Wu, and Q. Zhang, Gapless quantum spin liquid ground state in the two-dimensional spin-1/2 triangular antiferromagnet $YbMgGaO_4$, Sci. Rep. **5**, 16419 (2015).

[31] N. Elstner, R. R. P. Singh, and A. P. Young, Finite temperature properties of the spin-1/2 Heisenberg antiferromagnet on the triangular lattice, Phys. Rev. Lett. **71**, 1629 (1993).

[32] O. Mustonen, S. Vasala, E. Sadrollahi, K. P. Schmidt, C. Baines, H. C. Walker, I. Terasaki, F. J. Litterst, E. Baggio-Saitovitch, and M. Karppinen, Spin-liquid-like state in a spin-1/2 square-lattice antiferromagnet perovskite induced by $d^{10} - d^0$ cation mixing, Nat. Commun. **9**, 1085 (2018).

[33] Z. Zeng, X. Ma, S. Wu, H.-F. Li, Z. Tao, X. Lu, X. H. Chen, J.-X. Mi, S.-J. Song, G.-H. Cao, G. Che, K. Li, G. Li, H. Luo, Z. Y. Meng, and S. Li, Possible Dirac quantum spin liquid in the kagome quantum antiferromagnet $YCu_3(OH)_6Br_2[Br_x(OH)_{1-x}]$, Phys. Rev. B **105**, L121109 (2022).

[34] O. I. Motrunich, Variational study of triangular lattice spin-1/2 model with ring exchanges and spin liquid state in $\kappa-(ET)_2Cu_2CN_3$, Phys. Rev. B **72**, 045105 (2005).

[35] Y. Jana, A. Ghosal, S. Nandi, J. Alam, P. Bag, S. Islam, and R. Nath, Spin-ice behavior of mixed pyrochlore Dy_2GaSbO_7 exhibiting enhanced Pauling zero-point entropy, J. Magn. Magn. Mater. **562**, 169814 (2022).

[36] K. M. Ranjith, D. Dmytriieva, S. Khim, J. Sichelschmidt, S. Luther, D. Ehlers, H. Yasuoka, J. Wosnitza, A. A. Tsirlin, H. Kühne, and M. Baenitz, Field-induced instability of the quantum spin liquid ground state in the $J_{\text{eff}} = \frac{1}{2}$ triangular-lattice compound $NaYbO_2$, Phys. Rev. B **99**, 180401(R) (2019).

[37] V. K. Singh, K. Nam, M. Barik, K. Boya, E. Kermarrec, P. Khuntia, K. H. Kim, S. Bhowal, and B. Koteswararao, Bi_2YbO_4Cl: A two-dimensional square-lattice compound with $j_{\text{eff}} = \frac{1}{2}$ magnetic moments, Phys. Rev. B **109**, 075128 (2024).

[38] Y. Li, D. Adroja, P. K. Biswas, P. J. Baker, Q. Zhang, J. Liu, A. A. Tsirlin, P. Gegenwart, and Q. Zhang, Muon spin relaxation evidence for the U(1) quantum spin-liquid ground state in the triangular antiferromagnet $YbMgGaO_4$, Phys. Rev. Lett. **117**, 097201 (2016).

[39] S. Lee, C. H. Lee, A. Berlie, A. D. Hillier, D. T. Adroja, R. Zhong, R. J. Cava, Z. H. Jang, and K.-Y. Choi, Temporal and field evolution of spin excitations in the disorder-free triangular antiferromagnet $Na_2BaCo(PO_4)_2$, Phys. Rev. B **103**, 024413 (2021).

[40] Y. J. Uemura, A. Keren, K. Kojima, L. P. Le, G. M. Luke, W. D. Wu, Y. Ajiro, T. Asano, Y. Kuriyama, M. Mekata, H. Kikuchi, and K. Kakurai, Spin fluctuations in frustrated kagomé lattice system $SrCu_8Ga_4O_{19}$ studied by muon spin relaxation, Phys. Rev. Lett. **73**, 3306 (1994).

[41] C. P. Slichter, *Principles of Magnetic Resonance*, 3rd enlarged and updated edition, Springer Series in Solid-State Sciences (Springer, Berlin, 1989), pp. 449–450.

[42] D. Bono, P. Mendels, G. Collin, N. Blanchard, F. Bert, A. Amato, C. Baines, and A. D. Hillier, μSR study of the quantum dynamics in the frustrated $S = \frac{3}{2}$ kagomé bilayers, Phys. Rev. Lett. **93**, 187201 (2004).

[43] A. Keren, J. S. Gardner, G. Ehlers, A. Fukaya, E. Segal, and Y. J. Uemura, Dynamic properties of a diluted pyrochlore cooperative paramagnet $(Tb_pY_{1-p})_2Ti_2O_7$, Phys. Rev. Lett. **92**, 107204 (2004).

[44] Z. Zhang, J. Li, M. Xie, W. Zhuo, D. T. Adroja, P. J. Baker, T. G. Perring, A. Zhang, F. Jin, J. Ji, X. Wang, J. Ma, and Q. Zhang, Low-energy spin dynamics of the quantum spin liquid candidate $NaYbSe_2$, Phys. Rev. B **106**, 085115 (2022).

[45] E. Kermarrec, P. Mendels, F. Bert, R. H. Colman, A. S. Wills, P. Strobel, P. Bonville, A. Hillier, and A. Amato, Spin-liquid ground state in the frustrated kagome antiferromagnet $MgCu_3(OH)_6Cl_2$, Phys. Rev. B **84**, 100401(R) (2011).

[46] I. Ishant, T. Shiroka, O. Stockert, V. Fritsch, and M. Majumder, Frustration-induced quantum criticality in Ni-doped CePdAl as revealed by the μSR technique, Phys. Rev. Res. **6**, 023112 (2024).

[47] R. Sarkar, P. Schlender, V. Grinenko, E. Haeussler, P. J. Baker, T. Doert, and H.-H. Klauss, Quantum spin liquid ground state in the disorder free triangular lattice $NaYbS_2$, Phys. Rev. B **100**, 241116(R) (2019).

[48] C. Balz, B. Lake, J. Reuther, H. Luetkens, R. Schönemann, T. Herrmannsdörfer, Y. Singh, A. T. M. Nazmul Islam, E. M. Wheeler, J. A. Rodriguez-Rivera, T. Guidi, G. G. Simeoni, C. Baines, and H. Ryll, Physical realization of a quantum spin liquid based on a complex frustration mechanism, Nat. Phys. **12**, 942 (2016).

[49] R. Tripathi, D. T. Adroja, C. Ritter, S. Sharma, C. Yang, A. D. Hillier, M. M. Koza, F. Demmel, A. Sundaresan, S. Langridge, W. Higemoto, T. U. Ito, A. M. Strydom, G. B. G. Stenning, A. Bhattacharyya, D. Keen, H. C. Walker, R. S. Perry, F. Pratt, Q. Si, and T. Takabatake, Quantum critical spin-liquid-like behavior in the $S = \frac{1}{2}$ quasikagome-lattice compound $CeRh_{1-x}Pd_xSn$ investigated using muon spin relaxation and neutron scattering, Phys. Rev. B **106**, 064436 (2022).

[50] A. T. Ogielski, Dynamics of three-dimensional Ising spin glasses in thermal equilibrium, Phys. Rev. B **32**, 7384 (1985).

[51] I. A. Campbell, A. Amato, F. N. Gygax, D. Herlach, A. Schenck, R. Cywinski, and S. H. Kilcoyne, Dynamics in canonical spin glasses observed by muon spin depolarization, Phys. Rev. Lett. **72**, 1291 (1994).

[52] Y. J. Uemura, T. Yamazaki, D. R. Harshman, M. Senba, and E. J. Ansaldo, Muon-spin relaxation in *Au*Fe and *Cu*Mn spin glasses, Phys. Rev. B **31**, 546 (1985).

[53] H. Murayama, Y. Sato, T. Taniguchi, R. Kurihara, X. Z. Xing, W. Huang, S. Kasahara, Y. Kasahara, I. Kimchi, M. Yoshida, Y. Iwasa, Y. Mizukami, T. Shibauchi, M. Konczykowski, and Y. Matsuda, Effect of quenched disorder on the quantum spin liquid state of the triangular-lattice antiferromagnet $1T-TaS_2$, Phys. Rev. Res. **2**, 013099 (2020).

[54] H. Murayama, T. Tominaga, T. Asaba, A. de Olivira Silva, Y. Sato, H. Suzuki, Y. Ukai, S. Suetsugu, Y. Kasahara, R. Okuma, I. Kimchi, and Y. Matsuda, Universal scaling of specific heat in the $S = \frac{1}{2}$ quantum kagome antiferromagnet herbertsmithite, Phys. Rev. B **106**, 174406 (2022).

[55] I. Kimchi, J. P. Sheckelton, T. M. McQueen, and P. A. Lee, Scaling and data collapse from local moments in frustrated disordered quantum spin systems, Nat. Commun. **9**, 4367 (2018).

[56] M. Majumder *et al.*, Microscopic Investigation of the ground state of quantum spin liquid candidate $Sr_3CuTa_2O_9$, STFC ISIS Neutron and Muon Source (2024), https://doi.org/10.5286/ISIS.E.RB2368012.

[57] J. Rodríguez-Carvajal, Recent advances in magnetic structure determination by neutron powder diffraction, Phys. B: Condens. Matter **192**, 55 (1993).

[58] A. Suter and B. Wojek, Musrfit: A free platform-independent framework for μSr data analysis, Phys. Procedia **30**, 69 (2012).

[59] M. Tamura and R. Kato, Magnetic susceptibility of $\beta'[Pd(dmit)_2]$ salts (dmit=1,3-dithiol-2-thione-4,5-dithiolate, C_3S_5): Evidence for frustration in spin-1/2 Heisenberg antiferromagnets on a triangular lattice, J. Phys.: Condens. Matter **14**, L729 (2002).

[60] M. Yamashita, N. Nakata, Y. Senshu, M. Nagata, H. M. Yamamoto, R. Kato, T. Shibauchi, and Y. Matsuda, Highly mobile gapless excitations in a two-dimensional candidate quantum spin liquid, Science **328**, 1246 (2010).

[61] X. Hong, M. Gillig, R. Hentrich, W. Yao, V. Kocsis, A. R. Witte, T. Schreiner, D. Baumann, N. Pérez, A. U. B. Wolter, Y. Li, B. Büchner, and C. Hess, Strongly scattered phonon heat transport of the candidate Kitaev material $Na_2Co_2TeO_6$, Phys. Rev. B **104**, 144426 (2021).

[62] M. Li and G. Chen, Thermal transport for probing quantum materials, MRS Bull. **45**, 348 (2020).